Journal of Asian Ceramic Societies 4 (2016) 124–132

Contents lists available at ScienceDirect

Journal of Asian Ceramic Societies

journal homepage: www.elsevier.com/locate/jascer

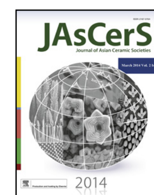

Structure, optical and electrical properties of indium tin oxide ultra thin films prepared by jet nebulizer spray pyrolysis technique

M. Thirumoorthi [a], J. Thomas Joseph Prakash [b,*]

[a] Department of Physics, H.H. The Rajah's College (Affiliated to Bharathidasan University), Pudukkottai 622001, India
[b] Department of Physics, Government Arts College (Affiliated to Bharathidasan University), Trichy 620 022, India

ARTICLE INFO

Article history:
Received 3 November 2015
Received in revised form
27 December 2015
Accepted 5 January 2016
Available online 20 January 2016

Keywords:
ITO thin films
Nebulizer spray pyrolysis
X-ray methods
Surfaces roughness
Electrical properties

ABSTRACT

Indium tin oxide (ITO) thin films have been prepared by jet nebulizer spray pyrolysis technique for different Sn concentrations on glass substrates. X-ray diffraction patterns reveal that all the films are polycrystalline of cubic structure with preferentially oriented along (222) plane. SEM images show that films exhibit uniform surface morphology with well-defined spherical particles. The EDX spectrum confirms the presence of In, Sn and O elements in prepared films. AFM result indicates that the surface roughness of the films is reduced as Sn doping. The optical transmittance of ITO thin films is improved from 77% to 87% in visible region and optical band gap is increased from 3.59 to 4.07 eV. Photoluminescence spectra show mainly three emissions peaks (UV, blue and green) and a shift observed in UV emission peak. The presence of functional groups and chemical bonding was analyzed by FTIR. Hall effect measurements show prepared films having n-type conductivity with low resistivity (3.9×10^{-4} Ω-cm) and high carrier concentrations (6.1×10^{20} cm^{-3}).

© 2016 The Ceramic Society of Japan and the Korean Ceramic Society. Production and hosting by Elsevier B.V. This is an open access article under the CC BY-NC-ND license (http://creativecommons.org/licenses/by-nc-nd/4.0/).

1. Introduction

Indium tin oxide (ITO) is a well known n-type transparent conducting oxide material. Here tin acts as a cationic dopant in the In_2O_3 lattice and as a substitute on the indium sites to bind with the interstitial oxygen. Due to its high optical transmittance, electrical conductivity and wide band gap (>3.5 eV), ITO has been widely applied in various optoelectronic devices such as photovoltaic cells [1], liquid crystal displays [2] and gas sensors [3]. The ITO thin films are commonly fabricated by employing different techniques such as magnetron sputtering [4–8], sol–gel process [9–11], thermal evaporation [12], pulsed laser deposition [13,14], chemical vapor deposition [15,16], spray pyrolysis [17–22] and nebulizer spray pyrolysis (NSP) [23]. All of these methods have advantages and disadvantages, but jet nebulizer spray pyrolysis has a noticeable advantage; it is a low-cost and non-vacuum technique for large area applications and can produce high quality film with low precursor volume. The working of NSP method is based on the Bernoulli principle; i.e., when a pressurized flow of air is directed through a constricted orifice, the velocity of the airflow is increased to create a jet stream. The impact of a jet stream with liquid produces aerosol particles (particle size ~2.5 μm) [24]. The mist form of solution is helping to improve the quality of film and to obtain a uniform growth due to gradual nucleation with minimum wastage. In the present study, the tin doped indium oxide thin films were prepared by a simple and low-cost jet nebulizer spray pyrolysis technique. The structure, surfaces, optical, photoluminescence and electrical properties of prepared films were investigated in detail.

2. Experiment

A jet nebulizer spray pyrolysis apparatus (Fig. 1) is used in this work, which consists of a jet nebulizer spraying unit, substrate holder with heater and air compressor. To prepare tin doped indium oxide thin films, the indium (III) chloride ($InCl_3$) is dissolved in 100 mL double distilled water to make 0.4 M starting solution. Tin doping was achieved by adding tin (II) chloride dihydrates ($SnCl_2{\cdot}2H_2O$) to the starting solution. A few drops of acetic acid were added to obtain a clear and homogeneous solution. The doping level in the solution was varied from 0 to 30 wt% in steps of 10 wt%. The mixture was stirred under constant speed for 1 h with a magnetic stirrer. Prior to the deposition, glass substrates (1 in.^{2}) were cleaned with acetone, isopropyl alcohol, and distilled water successively for 15 min in ultrasonicator. The substrate

* Corresponding author. Tel.: +91 9842470521.
E-mail address: armyjpr1@yahoo.co.in (J. Thomas Joseph Prakash).
Peer review under responsibility of The Ceramic Society of Japan and the Korean Ceramic Society.

http://dx.doi.org/10.1016/j.jascer.2016.01.001
2187-0764 © 2016 The Ceramic Society of Japan and the Korean Ceramic Society. Production and hosting by Elsevier B.V. This is an open access article under the CC BY-NC-ND license (http://creativecommons.org/licenses/by-nc-nd/4.0/).

Nomenclature

D	Crystallite size (nm)
k	Scherrer's constant
d	Lattice spacing (Å)
h,k,l	Miller indices
TC	Texture coefficient
$I_{(hkl)}$	Peak intensity
N	Number of peaks
T	Transmittance (%)
$h\nu$	Photon energy (eV)
E_g	Optical band gap (eV)
n	Carrier concentrations (cm^{-3})
β	Full width at half maximum (rad)
λ	Wavelength of X-ray (Å)
θ	Bragg's angle (deg)
ε	Strain
α	Absorption coefficient
ρ	Resistivity (Ω-cm)
μ	Mobility (cm/(V s))

temperature for each deposition was kept at 500 °C in the air atmosphere. The prepared solution was sprayed with a jet nebulizer (HUDSON RCI micro mist, droplet size is ∼2.7 μm) on the heated substrate with spray rate 0.5 mL/min using compressed air as a carrier gas. The nebulizer was kept at a distance of 5 cm from substrate surface.

The structural parameters of spray coated ITO films were analyzed by X-ray diffractometer (XRD) using the PANalytical system with Cu Kα_1 radiation (k = 1.54056 Å). Surface morphology and topography were carried out by the scanning electron microscope (ESEMQUANTA200, FEI-Netherlands) and atomic force microscopy (Agilent 5500) respectively. Elemental analysis was made by using energy dispersive X-ray spectroscopy (attached to SEM). The water contact angle measurement was made by using a protractor from microphotograph. The optical properties of the films were examined with a double beam spectrophotometer (Oceans optics HR2000-USA) in the UV–vis regions. The film thickness was measured by a profilometer (SJ-301 Mitutoyo). The photoluminescence (PL) spectra were recorded using a spectrofluorometer (Cary Eclipse EL08083851) with xenon arc lamp. The IR spectrum was recorded

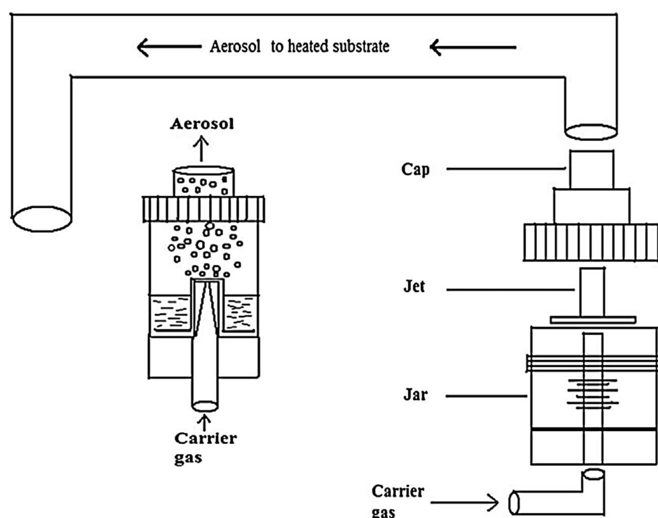

Fig. 1. Schematic diagram of jet nebulizer apparatus.

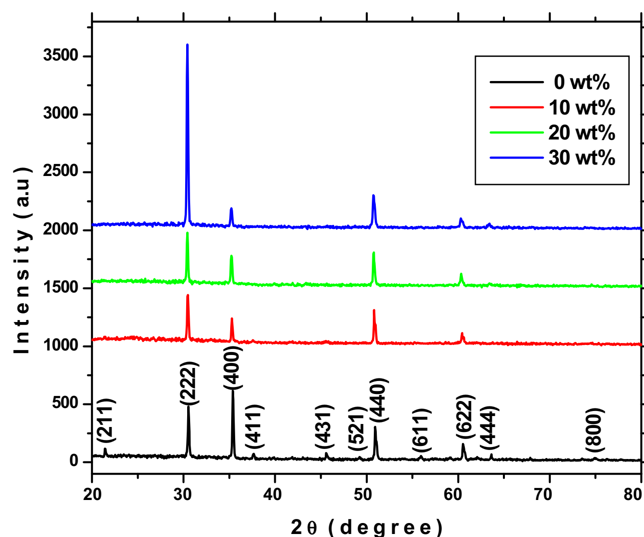

Fig. 2. X-ray diffraction patterns of ITO thin films for different Sn concentrations.

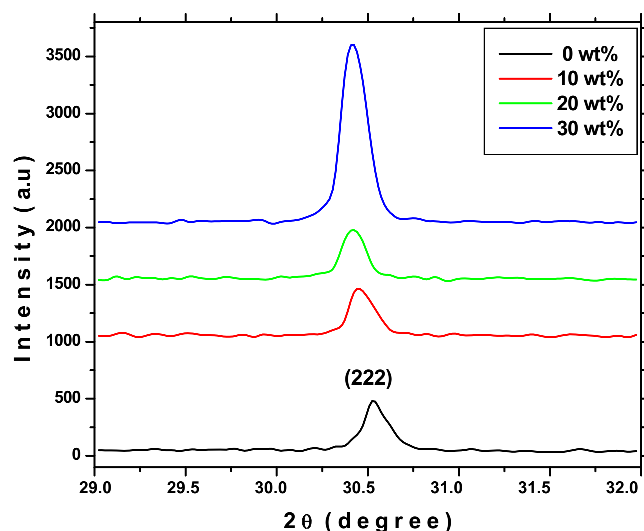

Fig. 3. Shift of peak position of ITO thin films along (222) plane for different Sn concentrations.

using FTIR spectrophotometer (Perkin Elmer – RX I) in the range of 400–4000 cm^{-1}. The electrical parameters were collected from room temperature Hall effect measurements (RH2035 PhysTech GmbH) system.

3. Results and discussion

3.1. Structural analysis

X-ray diffraction patterns are used to study the crystal structure of prepared ITO thin films. Fig. 2 shows the X-ray diffraction patterns of indium tin oxide thin films for different tin concentrations on glass substrates. It can be seen that all the films are polycrystalline in nature and crystallize in a cubic structure (JCPDS: 71-2194) with predominant (222) peak. A switching in the preferential growth from the (400) to (222) planes was observed when tin doped with indium oxide. The increasing intensity of the (222) plane is attributed to the increase in the degree of preferential crystal orientation. It is evident from the XRD spectra that no diffraction peaks of Sn or other impurity phases are detected in the prepared samples. As shown in Fig. 3 shift of the (222) peak toward smaller 2θ

Table 1
Structural parameters of prepared ITO thin films for different Sn concentrations.

Sample	2θ (deg)	hkl	FWHM (deg)	d-space (Å)		Crystallite size (nm)	Dislocation density, δ ($\times 10^{14}$ lines/m^2)	Strain, ε ($\times 10^{-4}$)	Lattice constant (Å)	TC
				Observed	Standard					
0 wt%	21.47	211	0.13	4.1354	4.1302	62.19	2.5855	5.573	10.1296	0.7347
	30.52	222	0.11	2.9266	2.9205	74.85	1.7849	4.631	10.1381	0.6047
	35.37	400	0.12	2.5356	2.5292	69.49	2.0708	4.988	10.1424	3.6168
	37.67	411	0.16	2.3859	2.3846	52.45	3.6350	6.609	10.1225	1.0069
	45.60	431	0.15	1.9877	1.9841	57.47	3.0298	6.034	10.1353	0.9044
	49.22	521	0.30	1.8497	1.8471	29.12	11.793	11.90	10.1312	0.5721
	50.94	440	0.12	1.7912	1.7884	73.34	1.8598	4.726	10.1325	1.4156
	55.92	611	0.26	1.6429	1.6411	34.59	8.3579	10.02	10.1275	0.7312
	60.57	622	0.16	1.5274	1.5252	57.48	3.0266	6.030	10.1316	0.1023
	63.68	444	0.27	1.4601	1.4602	34.63	8.3386	10.01	10.1158	0.2796
	75.02	800	0.19	1.2651	1.2646	52.71	3.5992	6.576	10.1201	1.0416
	Average					**54.3927**				
10 wt%	30.47	222	0.11	2.9313	2.9205	74.84	1.7853	4.632	10.1543	1.5071
	35.32	400	0.17	2.5391	2.5292	49.03	4.1592	7.070	10.1564	1.1216
	50.87	440	0.19	1.7935	1.7884	46.28	4.6688	7.489	10.1455	0.6831
	60.47	622	0.21	1.5297	1.5252	43.76	5.2221	7.920	10.1468	0.6883
	Average					**53.4775**				
20 wt%	30.42	222	0.11	2.9360	2.9205	74.84	1.7853	4.631	10.1706	1.4303
	35.42	400	0.13	2.5391	2.5292	64.13	2.4315	5.405	10.1564	1.3201
	50.80	440	0.13	1.7958	1.7884	67.64	2.1857	5.124	10.1585	0.6223
	60.35	622	0.17	1.5324	1.5252	54.11	3.4154	6.413	10.1647	0.6271
	Average					**65.18**				
30 wt%	30.37	222	0.11	2.9407	2.9205	74.85	1.7849	4.631	10.1868	1.9836
	35.25	400	0.11	2.5440	2.5292	75.78	1.7413	4.574	10.1761	1.0333
	50.79	440	0.12	1.7961	1.7884	73.31	1.8606	4.728	10.1602	0.6046
	60.38	622	0.13	1.5397	1.5252	70.72	1.9994	4.901	10.2132	0.4345
	Average					**73.665**				

value is due to the replacement of smaller radius Sn^{4+} ion (0.71 Å) in indium sites and also related to changes of strain in the crystal lattice [25].

The crystallite size was calculated from the XRD pattern using Debye-Scherrer formula [26]:

$$D = \frac{0.9\lambda}{\beta\cos\theta}, \quad (1)$$

where λ is X-ray wavelength (λ = 1.54060 Å), β is full width at half maximum in radian and θ is Bragg's angle.

The dislocation density (δ) and strain (ε) were calculated using the following equations [26]:

$$\delta = \frac{1}{D^2} \quad (2)$$

$$\varepsilon = \frac{\beta\cos\theta}{4} \quad (3)$$

Texture coefficient (TC) measures the relative degree of preferred orientation among crystal planes, which is obtained from following expression [27]:

$$TC_{(hkl)} = \left[\frac{I_{(hkl)}/I_{o\,(hkl)}}{N^{-1}\sum_N (I_{(hkl)}/I_{o\,(hkl)})}\right] \quad (4)$$

where $I_{(hkl)}$ is the measured intensity of the plane (*hkl*), $I_{o\,(hkl)}$ is the standard intensity of the respective diffraction plane, according to the JCPDS data card (71-2194) and N is the number of diffraction peaks presented.

The calculated structural parameters of prepared ITO thin films using the above equations are listed in Table 1. The observed improvement in average crystallite size is attributed to strain formed in the nano crystal. The dislocation density (δ) is to measure the disorder of lattice planes in the crystal structure. The strain arises due to point defects (vacancies, site disorder), dislocations and extended defects in the crystal structures. The calculated values of the lattice constant '*a*' are in good agreement with standard values (71-2194). Obtained lattice constant values are slightly increased for (222) plane with increased doping level, which can be related to uniform-strain of the grains. The texture coefficient TC (*hkl*) values calculated for the different planes of the films are shown in Table 1. The results indicate that the preferential orientation for pure indium oxide film along (400) plane, is shifted to (222) plane for Sn doped indium oxide films. The change of preferred orientation may be due to occupancy of additional indium vacancy sites by tin atoms which are unoccupied previously. In fact, it is well known that In_2O_3 thin films have several defect levels such as indium interstitial oxygen and indium vacancies [28]. The increase in preferred orientation is associated with the increase of crystallite growth along that plane. The change in peak intensity, *d*-value, lattice constants and strain confirms the substitution of Sn into In–O lattice.

3.2. Surface morphological analysis

For thin films the surface morphology depends on the deposition technique and its parameters. The surface morphology may influence the film properties such as mechanical, electrical and optical properties. Fig. 4 shows the scanning electron microscopic images of ITO films for different Sn concentrations deposited on glass substrates. It can be seen that all the films have a uniform surface morphology consisting of spherical particles without any voids and cracks. The lowering grain boundary and large active surface help to improve the electrical conductivity and optical transmittance.

Energy dispersive X-ray spectroscopy (EDX) is an analytical technique used for the elemental analysis of a sample. The EDX spectra of the prepared ITO thin films are shown in Fig. 5. The spectra reveal that the presence of In, O and Sn elements in the deposited

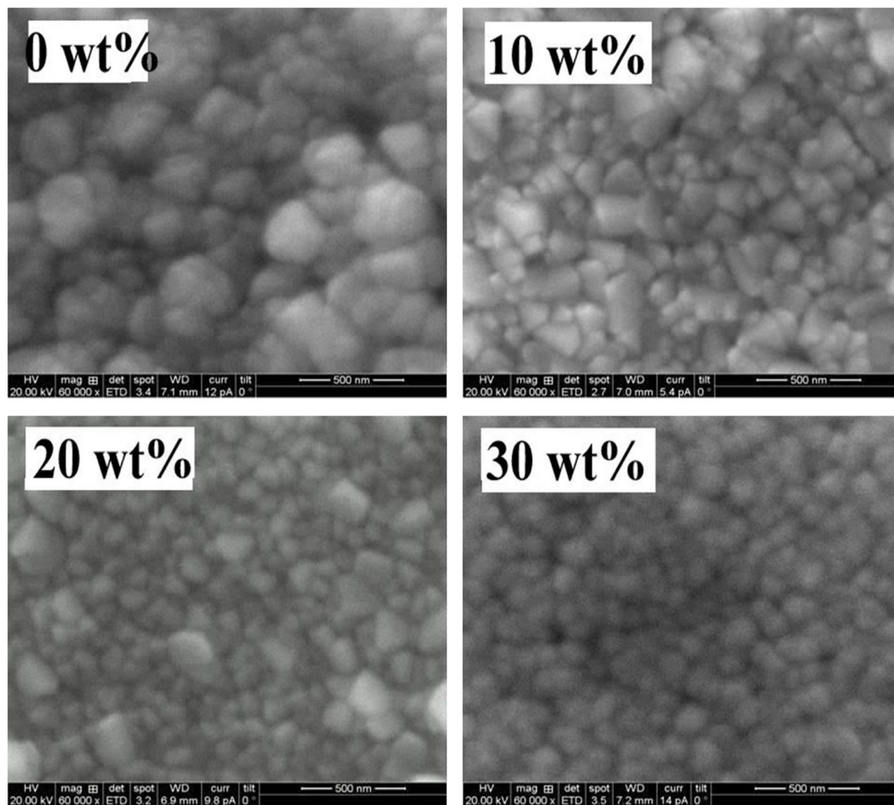

Fig. 4. Scanning electron microscopy images (60,000× magnification) of prepared ITO thin films.

films. The weight percentage is almost nearly equal to their nominal stoichiometry within the experimental error.

Topography is one of the most important physical characteristics of surfaces, which influence their significant technical properties. Fig. 6 shows the 3D-AFM images of prepared ITO thin films for different Sn concentrations. The un-doped indium oxide film has a large difference between peak and valley than Sn doped films. As shown in Table 2 the surface profile parameters are changed with increasing Sn concentration. The surface roughness (Sa) and root mean square (RMS) (Sq) values are reduced as increasing Sn concentrations. The obtained RMS value of ITO films is lower than the prepared one by other techniques such as ink-jet printing

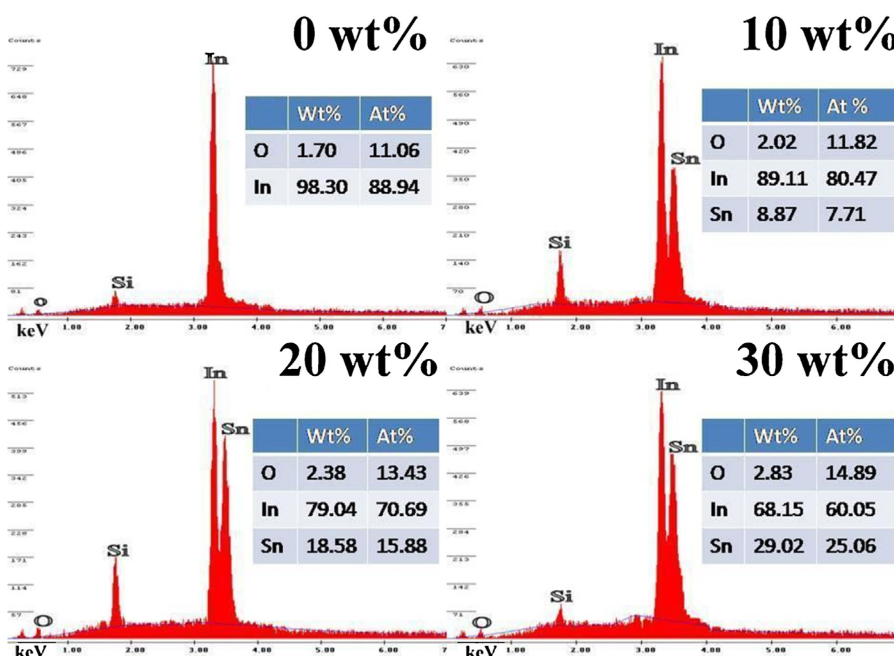

Fig. 5. Energy dispersive X-ray spectra of ITO thin films.

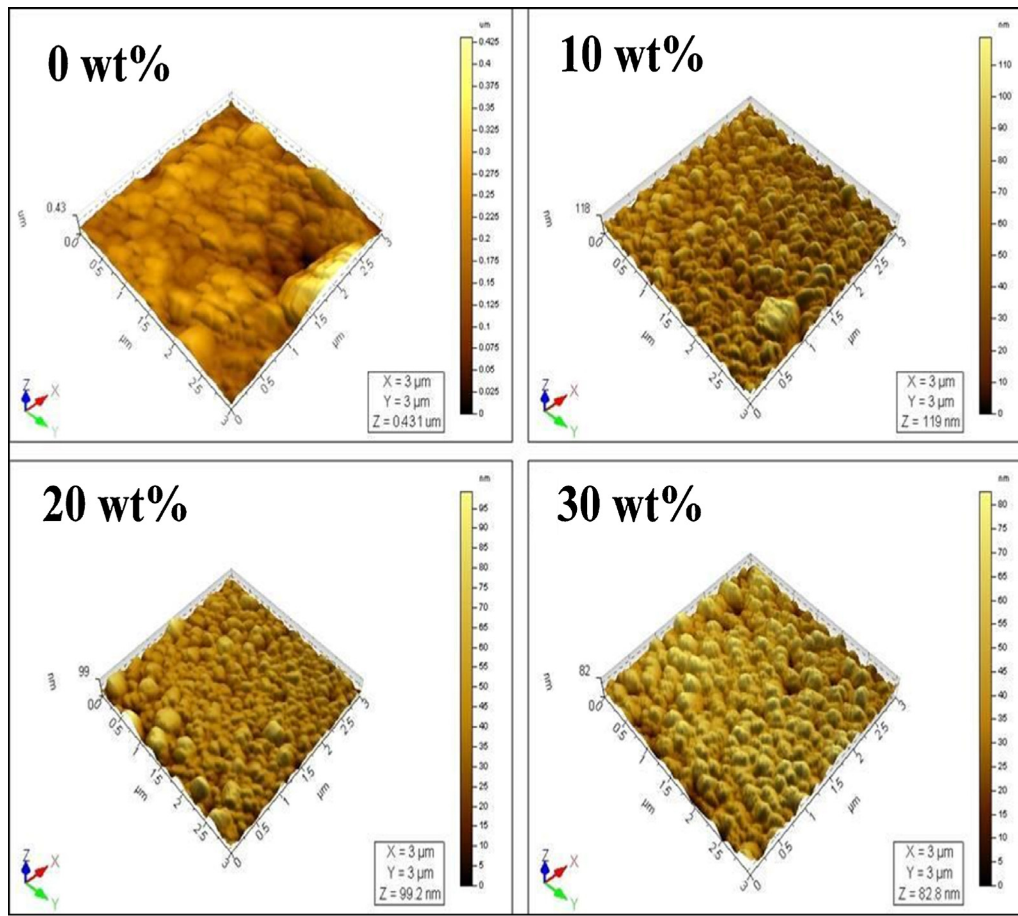

Fig. 6. AFM 3D images of prepared ITO thin films for different Sn concentrations.

[29], RF sputtering [30], chemical vapor deposition [31] and spray pyrolysis [32]. The average roughness is the mean value of peak and valley as calculated over the measured entire surface area. It is useful for detecting general variations in overall profile height characteristics. Root mean square roughness is the square root of the distribution of surface height and is considered to be more sensitive than the average roughness. It represents the standard deviation of the profile heights and is used in the computations of skewness and kurtosis. Surface skewness (Ssk) is used to measure the symmetry of the variations of surface about the mean line and is more sensitive to occasional deep valleys or high peaks. Surface kurtosis (Sku) is used to measure the distribution of the spikes above and below the mean line. The roughness reduction of the films helps to reduce the scattering of incident light and leading to increase of optical transmittance.

Fig. 7 shows the microphotographs of water droplet on the ITO surface, and thus it can be perceived that the water contact angles (127°, 114°, 106° and 92° for 0, 10, 20 and 30 wt% respectively) are decreased. This result indicates that the hydrophilicities of ITO surface are increased with Sn doping concentrations, and such a behavior is due to reduction of surface roughness.

3.3. Optical studies

The optical properties of thin films are known to depend strongly on the film thickness, microstructures, levels of impurities and deposition parameters. Fig. 8 shows the optical transmittance and the absorption spectrum of prepared ITO thin films for different doping concentrations. It is found that the average transmittance of the pure indium oxide film is 77% and that of the Sn doped films could be in the range of 82–87%, and such results may be related to low scattering of light and thickness. As shown in Fig. 8 (inset) the absorption edge is shifted to lower wavelength for Sn doped indium oxide films. The transmission spectra show just the opposite trend of the optical absorption spectra. The absorption of all the films is

Table 2
Height parameters of ITO thin film obtained from AFM analysis.

Parameters	0 wt%	10 wt%	20 wt%	30 wt%
Root mean square (Sq) (nm)	20.2	15.3	11	12
Surface Skewness (Ssk)	0.455	0.244	0.468	0.106
Coefficient of kurtosis (Sku)	5.21	3.27	4.25	2.85
Maximum peak height (Sp) (nm)	137	63.5	55.7	47.2
Ten point mean height (Sz) (nm)	431	119	99.5	82.8
Average surface roughness (Sa) (nm)	17.6	12.1	8.29	9.58
Film thickness (nm)	96	43	37	32

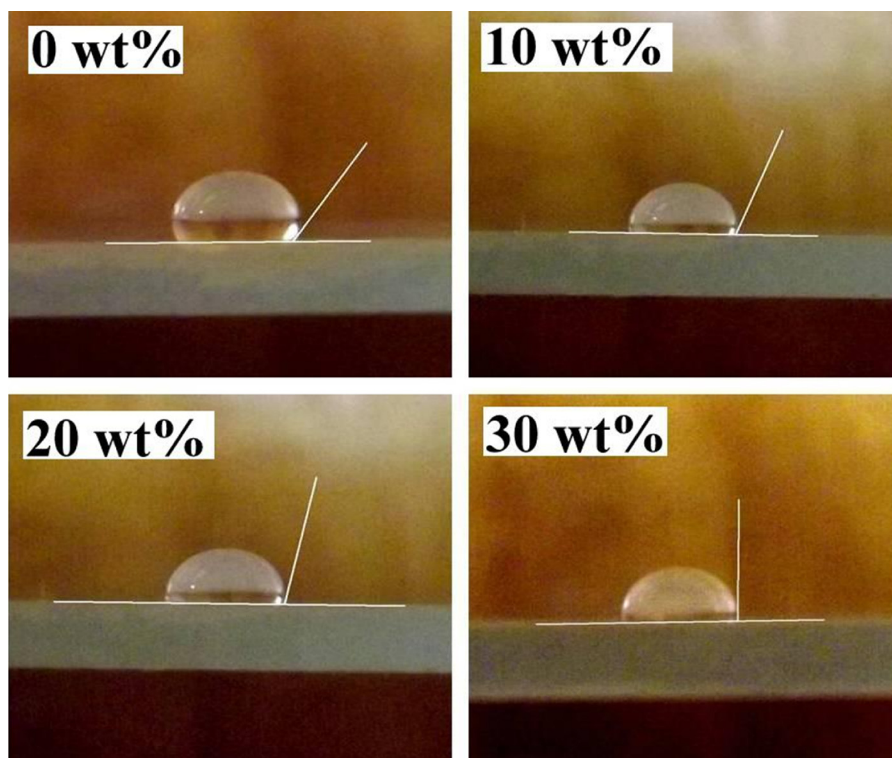

Fig. 7. Microphotographs of water droplet on ITO surface.

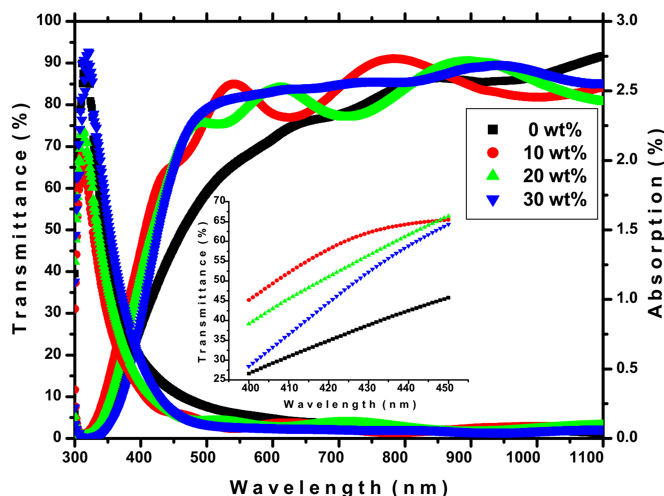

Fig. 8. UV–vis transmittance and absorption spectrum of ITO thin films. Inserted image shows the blue shift of absorption edges.

in the range of 0.04–1.10% in the visible region, the low absorption of incident light is essential for TCO.

The optical band gap (E_g) values calculated from the plot of $(\alpha h\nu)^2$ versus $(h\nu)$ is shown in Fig. 9(a)–(d) for the prepared films. The absorption coefficient (α) is calculated from the following relation [26]:

$$\alpha = \left(\frac{1}{d}\right) \ln \left(\frac{1}{T}\right) \tag{5}$$

where d is thickness of the films and T is transmittance. The absorption coefficient (α) and incident photon energy ($h\nu$) is related by the following relation [26]:

$$(\alpha h\nu)^2 = A(h\nu - E_g) \tag{6}$$

where A is a constant, $h\nu$ is photon energy and E_g is optical band gap. Obtained band gaps are plotted as a function of Sn concentrations that are shown in Fig. 9(e). It is observed that band gap increases rapidly from 3.59 eV (0 wt%) to 4.07 eV (10 wt%) and then decreased slightly to 4.01 eV (30 wt%). Similar behavior of band gap widening and then narrowing for higher doping of tin is reported previously by Benamar et al. [20]. The widening of the optical band gap is related to increased carrier concentration and which is explained by using Moss–Burstein effect [33]. The narrowing of band gap for higher Sn doping may be due to many-body interaction effects either between free carriers or between free carriers and ionized impurities [34].

3.4. Photoluminescence studies

The room temperature photoluminescence (PL) spectroscopy technique is a selective and extremely sensitive probe of discrete electronic states. Fig. 10 shows the room temperature PL spectra of ITO thin films recorded under the excitation wavelength λ = 310 nm. Mainly three emission peaks are observed as follows: a strong UV emission peak (P_1 at 363 nm), a strong blue emission peak (P_2 at 493 nm) and a weak green emission peak (P_3 at 521 nm). The UV emission peak is also called near band edge (NBE) emission, and it originates due to the recombination of the free exciton through an exciton–exciton collision process [35]. As shown in Fig. 10 (inset) a change observed in the UV emissions peak indicated that the recombination centers are modified by Sn doping. A blue emission band indicated that a new defect level is introduced into the band gap by the Sn doping [36]. The origin of green emission is generally ascribed to deep level defects such as surface defects and singly ionized oxygen vacancies [37]. A rapid decrease in the intensity of all peaks and the change of UV emission peak position confirm the substitution of Sn atom in indium sites.

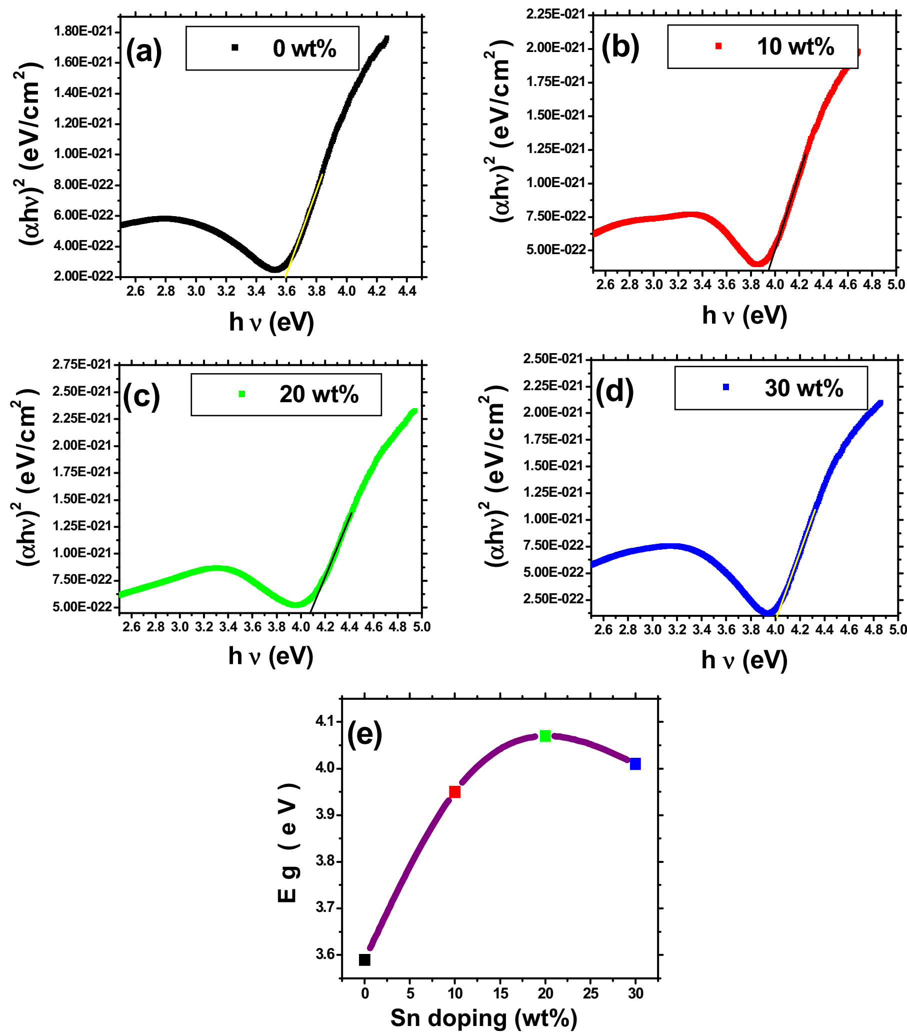

Fig. 9. (a–d) The $(\alpha h\nu)^2$ versus $h\nu$ plots of ITO thin films for different Sn concentrations; (e) variations of optical band gap as function of Sn concentrations.

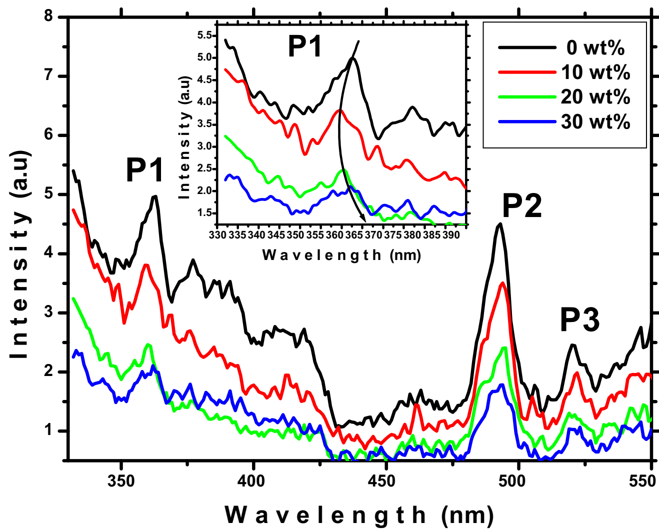

Fig. 10. Room temperature photoluminescence (PL) spectrum of ITO thin films; (insert) the observed change of UV emissions peaks position.

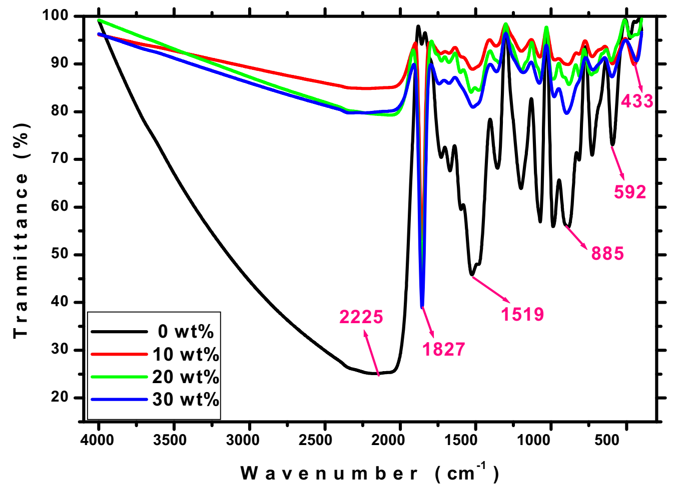

Fig. 11. FTIR spectra of ITO thin films for different Sn concentrations in wave number range from 400 to 4000 cm^{-1} at room temperature.

3.5. FTIR analysis

FTIR technique is used to obtain information about the chemical bonding and the presence of certain functional groups in a material. Fig. 11 shows the FTIR spectra of prepared ITO thin films for different Sn concentrations. The broad band around 3500–1900 cm^{-1} is attributed to the O—H stretching vibrations of hydroxyls from absorbing water molecules [38]. We can also recognize the strong absorption band at 1827 cm^{-1} is related to

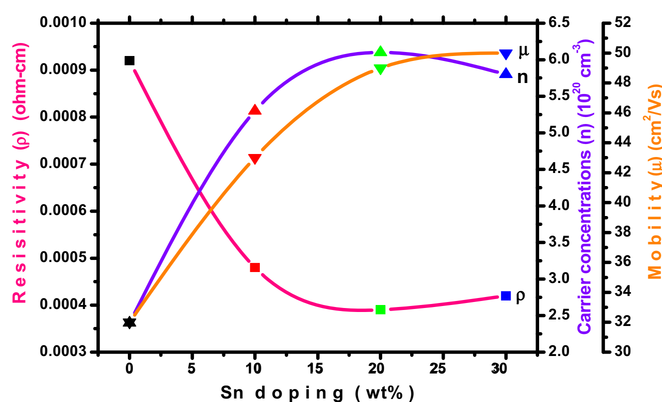

Fig. 12. Electrical parameters of prepared ITO thin films as function of Sn concentrations.

C═O stretching vibration of carboxylic acids, a medium band at 1519 cm^{-1} is related to C═C stretching vibration of arenes and a medium band at 885 cm^{-1} is ascribed to C—H bending vibration. The weak bands at 592 cm^{-1} and 433 cm^{-1} are attributed to In—O bond [39].

3.6. Electrical studies

Fig. 12 shows the measured electrical parameters of prepared ITO thin films as a function of different Sn concentrations. It can be seen that the resistivity is decreased, carrier concentration is increased and mobility is increased as increasing Sn concentrations, and this behavior is desirable for transparent conducting oxide. The results indicate that the prepared ITO thin films are highly degenerating n-type conductivity. The increase of carrier concentration value of ITO film is due to the valence difference between Sn^{4+} and In^{3+} ions, which generates extra one free carrier per atomic substitution and leading to decrease of resistivity. The incorporation of Sn dopant in indium oxide films changes the overall electrical properties significantly. We obtained a minimum electrical resistivity (3.9×10^{-4} Ω-cm) and maximum carrier concentration (6.1×10^{20} cm^{-3}) for 20 wt% of tin doped indium oxide thin film. Similar results were reported in previous literature by Seki et al. [40]. The increase of mobility is related to reduction of grain boundary scattering. The electronic transport property for the ultrathin films is entirely related to the microstructure of the films and doping concentration.

4. Conclusions

Transparent conducting indium tin oxide (ITO) thin films were successfully prepared by jet nebulizer spray pyrolysis technique. Effects of Sn doping concentrations on structure, surface, optical, photoluminescence and electrical properties were investigated. The following conclusions are derived after these investigations:

- The XRD patterns revealed that prepared ITO films are polycrystalline in nature with cubic structure. We observed a shift of preferential growth from (400) plane for pure indium oxide to (222) plane for Sn doped indium oxide thin films. The change observed in the peak position of (222) plane and structural parameters confirms the substitutions of Sn in In–O lattice.
- SEM images show the uniform distribution of spherical particles and the surface morphology also changed with Sn doping.
- The EDX spectrum reveals the presence of In, O and Sn elements in the deposited films with their nominal percentage.
- According to the 3D-AFM images the surface topography of the films is better than undoped films. The roughness and root mean square values are reduced as increased Sn concentrations.
- Optical transmissions of the films have improved from 77% to 87% and show an opposite trend of the optical absorption results. The observed initial blue shift in energy band gap from 3.59 to 4.07 eV can be explained by the Burstein–Moss effect.
- The decreasing photoluminescence peak intensity and observed shift in UV emissions peak positions is indicating the substitution of Sn in In–O system.
- The presence of functional groups and chemical bonding was confirmed by FTIR.
- Hall effect measurements show that Sn doping in indium oxide films effectively increases the carrier concentration and reduces its resistivity with an improvement in the mobility.

From these findings, we conclude that ITO thin films are suitable for optoelectronic applications and the jet nebulizer spray pyrolysis technique is suitable for producing uniform thin films with good quality.

References

[1] B.G. Lewis and D.C. Paine, MRS Bull., 25, 22–27 (2000).
[2] J.C. Manifacier, Thin Solid Films, 90, 297–307 (1982).
[3] G. Neri, A. Bonavita, G. Micali, G. Rizzo, E. Callone and G. Carturan, Sens. Actuators B, 132, 224–233 (2008).
[4] J.H. Park, C. Buurma, S. Sivananthan, R. Kodama, W. Gao and T.A. Gessert, Appl. Surf. Sci., 307, 388–392 (2014).
[5] K.-S. Tseng and Y.-L. Lo, Appl. Surf. Sci., 285P, 157–166 (2013).
[6] K.C. Heo, Y.k. Sohn and J.S. Gwag, Ceram. Int., 41, 617–621 (2015).
[7] Y.S. Jung, D.W. Lee and D.Y. Jeon, Appl. Surf. Sci., 221, 136–142 (2004).
[8] A. Klo Eppel, W. Kriegseis, B.K. Meyer, A. Scharmann, C. Daube, J. Stollenwerk and J. Trube, Thin Solid Films, 365, 139–146 (2000).
[9] Y. Wang, J. Liu, X. Wu and B. Yang, Appl. Surf. Sci., 308, 341–346 (2014).
[10] M.T. Kesim and C. Durucan, Thin Solid Films, 545, 56–63 (2013).
[11] L. Korosi, S. Korosi and I. Dekany, Thin Solid Films, 519, 3113–3118 (2011).
[12] K.-Y. Pan, L.-D. Lin, L.-W. Chang and H.C. Shih, Appl. Surf. Sci., 273, 12–18 (2013).
[13] J.B. Choi, J.H. Kim, K.A. Jeon and S.Y. Lee, Mater. Sci. Eng. B, 102, 376–379 (2003).
[14] J.M. Dekkers, G. Rijnders and D.H.A. Blank, Appl. Phys. Lett., 88, 151908 (2006).
[15] Y.C. Park, Y.S. Kim, H.K. Seo, S.G. Ansari and H.S. Shin, Surf. Coat. Technol., 161, 62–69 (2002).
[16] Y.S. Kim, Y.C. Park, S.G. Ansari, B.S. Lee and H.S. Shin, Thin Solid Films, 426, 124–131 (2003).
[17] V. Brinzari, I. Damaskin, L. Trakhtenberg, B.K. Cho and G. Korotcenkov, Thin Solid Films, 552, 225–231 (2014).
[18] P.K. Manoj, B. Joseph, V.K. Vaidyan and D. Sumangala Devi Amma, Ceram. Int., 33, 273–278 (2007).
[19] H. El Rhaleb, E. Benamar, M. Rami, J.P. Roger, A. Hakam and A. Ennaoui, Appl. Surf. Sci., 201, 138–145 (2002).
[20] E. Benamar, M. Rami, C. Messaoudi, D. Sayah and A. Ennaoui, Sol. Energy Mater. Sol. Cells, 56, 125–139 (1999).
[21] A.R. Babar, S.S. Shinde, A.V. Moholkar, C.H. Bhosale, J.H. Kim and K.Y. Rajpure, J. Alloys Compd., 509, 3108–3115 (2011).
[22] K. Ravichandran and K. Thirumurugan, J. Mater. Sci. Technol., 30, (2) 97–102 (2014).
[23] S. Marikkannu, M. Kashif, N. Sethupathy, V.S. Vidhya, S. Piraman, A. Ayeshamariam, M. Bououdina, N.M. Ahmed and M. Jayachandran, Mater. Sci. Semicond. Process., 27, 562–568 (2014).
[24] V. Gowthami, M. Meenakshi, P. Perumal, R. Sivakuma and C. Sanjeeviraja, Mater. Sci. Semicond. Process., 27, 1042–1049 (2014).
[25] G.B. Gonzalez, J.B. Cohen, J.H. Hwang, T.O. Mason, J.P. Hodges and J.D. Jorgensen, J. Appl. Phys., 89, 2550–2555 (2001).
[26] M. Thirumoorthi and J. Thomas Joseph Prakash, Superlattices Microstruct., 85, 237–247 (2015).
[27] S.S. Shinde, P.S. Shinde, S.M. Pawar, A.V. Moholkar, C.H. Bhosale and K.Y. Rajpure, Solid State Sci., 10, 1209–1214 (2008).
[28] Y.-R. Lyu and T.-E. Hsieh, Surf. Coat. Technol., 231, 219–223 (2013).
[29] H.-Y. Lai, T.-H. Chen and C.-H. Chen, Mater. Lett., 65, 3336–3339 (2011).
[30] T. Konry and R.S. Marks, Thin Solid Films, 492, 313–321 (2005).
[31] N. Wolf, M. Rydzek, D. Gerstenlauer, M. Arduini-Schuster and J. Manara, Thin Solid Films, 532, 60–65 (2013).
[32] E.S. Raj and K.L. Choy, Mater. Chem. Phys., 82, 489–492 (2003).
[33] E. Burstein, Phys. Rev., 93, 632–701 (1954).
[34] A. Walsh, J.L.F. Da Silva and S.-H. Wei, Phys. Rev. B, 78, 075211 (2008).
[35] A. Umar, B. Karunagaran, E.K. Suh and Y.B. Hahn, Nanotechnology, 17, 4072–4079 (2006).

[36] Y.A. Cao, W.S. Yang, W.F. Zhang, G.Z. Liu and P.L. Yue, New J. Chem., 28, 218–222 (2004).
[37] Y. Li, Y. Bando and D. Golberg, Adv. Mater., 15, 581–585 (2003).
[38] R.J. Keller, The Sigma Library of FTIR Spectra, vol. 2, Sigma Chemical, St. Louis (1986).
[39] R.A. Nyquist and R.O. Kagel, Infrared Spectra of Inorganic Compounds, vol. 4, Academic Press, New York (1971).
[40] S. Seki, Y. Sawada, M. Ogawa, M. Yamamoto, Y. Kagota, A. Shida and M. Ide, Surf. Coat. Technol., 169–170, 525–527 (2003).